NAVAL POSTGRADUATE SCHOOL
Monterey, California

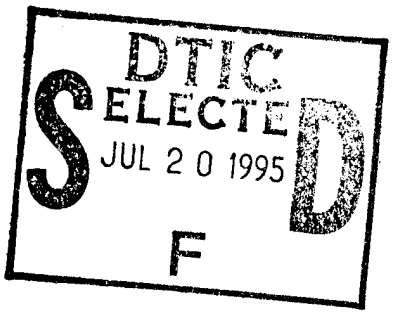

THESIS

WAVELENGTH MODULATION IN FREE ELECTRON LASERS

by

W. Randall Pinkley

March 1995

Thesis Advisor: W.B. Colson

JGK

REPORT DOCUMENTATION PAGE

Form Approved
OMB No. 0704-0188

1. AGENCY USE ONLY *(Leave blank)*	2. REPORT DATE	3. REPORT TYPE AND DATES COVERED
	March 1995	Master's Thesis

4. TITLE AND SUBTITLE
Wavelength Modulation in Free Electron Lasers

5. FUNDING NUMBERS

6. AUTHOR(S)
W.R. Pinkley

7. PERFORMING ORGANIZATION NAME(S) AND ADDRESS(ES)
Naval Postgraduate School
Monterey, CA 93943-5000

8. PERFORMING ORGANIZATION REPORT NUMBER

9. SPONSORING/MONITORING AGENCY NAME(S) AND ADDRESS(ES)
Naval Postgraduate School
Monterey, CA 93943-5000

10. SPONSORING/MONITORING AGENCY REPORT NUMBER

11. SUPPLEMENTARY NOTES
The views expressed in this thesis are those of the author and do not reflect the official policy of the Department of Defense or the U.S. Government.

12a. DISTRIBUTION/AVAILABILITY STATEMENT
Approved for public release; distribution unlimited.

12b. DISTRIBUTION CODE

13. ABSTRACT *(Maximum 200 words)*

The optical wavelength of a Free Electron Laser (FEL) is dependent on the input electron beam energy. So, as the energy of this beam varies, the optical wavelength from the laser wil vary as well. In many applications, this effect may be unwanted and in others it may be desirable. At the Stanford University Superconducting Free Electron Laser Facility, a feedback mechanism has been implemented to study the effects of electron beam energy fluctuation. Here, numerical techniques are used to study optical wavelength modulation caused by electron beam energy modulation where the amplitude modulation is within the gain spectrum bandwidth of the FEL.

14. SUBJECT TERMS
FEL, Free Electron Laser, short pulse simulation, resonant wavelength modulation, optical phase progression, limit cycles.

15. NUMBER OF PAGES
54

16. PRICE CODE

17. SECURITY CLASSIFICATION OF REPORT	18. SECURITY CLASSIFICATION OF THIS PAGE	19. SECURITY CLASSIFICATION OF ABSTRACT	20. LIMITATION OF ABSTRACT
UNCLASSIFIED	UNCLASSIFIED	UNCLASSIFIED	UL

NSN 7540-01-280-5500

Standard Form 298 (Rev 2-89)
Prescribed by ANSI Std Z39-18
298-102

Approved for public release: distribution is unlimited.

WAVELENGTH MODULATION IN FREE ELECTRON LASERS

W. R. Pinkley

Lieutenant, United States Navy

B.S., University of Central Florida, 1986

Submitted in partial fulfillment of the

requirements for the degree of

MASTER OF SCIENCE IN PHYSICS

from the

NAVAL POSTGRADUATE SCHOOL

March 1995

Author: W. Randall Pinkley

Approved by: W. B. Colson

William B. Colson, Thesis Advisor

Robert L. Armstead

Robert L. Armstead, Second Reader

W. B. Colson

William B. Colson, Chairman,

Department of Physics

ABSTRACT

The optical wavelength of a Free Electron Laser (FEL) is dependent on the input electron beam energy. So, as the energy of this beam varies, the optical wavelength from the laser will vary as well. In many applications, this effect may be unwanted and in others it may be desirable. At the Stanford University Superconducting Free Electron Laser Facility, a feedback mechanism has been implemented to study the effects of electron beam energy fluctuation. Here, numerical techniques are used to study optical wavelength modulation caused by electron beam energy modulation where the amplitude modulation is within the gain spectrum bandwidth of the FEL.

TABLE OF CONTENTS

ACKNOWLEDGEMENT

The author is grateful to the Naval Postgraduate School for support of this work. The author would also like to thank W. B. Colson for his invaluable assistance and guidance, R. L. Armstead for meticulous attention to detail as second reader, Robert Wong for his insight and technical assistance, and Jennifer Wanke for her faith and moral support.

I. INTRODUCTION

A. THE CASE FOR THE LASER IN DEFENSE

With the firing of Soviet made Scud missiles at Coalition forces and the nation of Israel during the Gulf War of 1991, it became painfully apparent that the U.S. was without a sufficiently capable weapon system to counter the threat of Theatre Ballistic Missiles on a consistent basis. The Patriot missile system was initially touted as the 'savior' of the day during Operation Desert Storm, but after further thought it seemed that the Patriot might not have been enough if the incoming missiles had been armed with NBC (nuclear, biological, or chemical) warheads. It was even put forward that the effect of the missiles would have been less severe if it hadn't been broken into many potentially lethal large pieces. Clearly, something was needed that could defeat the ballistic missile before it entered the terminal phase of its trajectory. With the dismal failure to locate a single missile site before the launch of a Scud missile, and the prospect of missile sites in future engagements being even harder to detect due to terrain or movement, the logical choice is a system to engage the ballistic missile during its boost and/or early post-boost phase of flight. The laser may be a suitable candidate for this purpose and has indeed been tested in the anti-missile role [1].

Another shortcoming during Operation Desert Storm was the failure to clear the operations area of the Persian Gulf of mines before two ships were damaged by anti-ship mines (the USS Tripoli and the USS Antietem) while conducting operations off the Kuwait/Iraq coast. Not only was this a serious threat to any attempt to liberate Kuwait from the sea, it made normal patrol and logistic support a dangerous proposition. Again, something more was needed to counter this threat. Actually, a laser system was tested during Operation Desert

Shield/Storm under the project name Magic Lantern. More work needs to be done to fully realize the potential of this type of system [2].

Fortunately, there were no incidents of Coalition Force surface units being attacked by missiles. While the multi-layered defense currently employed surely would have worked well against this threat, the possibility of 'leakers' through this 'net' cannot be discounted. It may be that the Vulcan/Phalanx Close In Weapons System might not be adequate to totally defeat this threat. Due to a significant dispersion of projectiles, there is a degradation in expected performance. The shortened range from the ship at which these missiles would be destroyed could leave the ship in serious danger from the fragments left over from the destruction of the missiles. The laser would provide a possible answer to this dilemma. With sufficient power, the laser could assure destruction of the incoming missiles at a range where the fragments from the missiles wouldn't pose a threat to the target ship.

B. A SHORT HISTORY OF THE FREE ELECTRON LASER

The Free Electron Laser traces its origins to 1951 when Hans Motz proposed the wiggler magnet used in current FEL designs. Demonstration of incoherent radiation in the millimeter and optical regions was subsequently shown by Motz in 1953. An increase in electron density was implemented in the 'ubitron' design put forth by Robert M. Phillips, which obtained high power (>1 MW) and efficiency (>10%) in wavelengths from 10cm to 5mm. The traveling-wave tube, which was developed around the same time, offered better performance and the ubitron was shelved temporarily.

In 1971, John M. J. Madey of Stanford University brought attention to what he proposed as the 'free-electron laser'. Relying on research of synchrotron-radiation sources, Madey conceived a device which would lase in the visible using relativistic electrons as the source. Initially, the free-electron laser was described

with quantum-mechanical theory, but later proposals made it clear that classical methods could be used instead. This was a large step in FEL design and allowed for much more effectual methods of describing the FEL.

The obvious potential for a tunable laser of high power brought widespread interest in many countries. It wasn't until six years later that a FEL was operated in the visible range. Gain in a FEL was demonstrated by Madey in 1976, a year after which lasing in the visible was achieved by the same team, and the race was on to build better designs. Three other FEL designs soon followed. The first was at Laboratoire pour l'Utilisation du Rayonment Electromagnetique in Orsay, France, which operated in the visible. The second involved a team from TRW at Stanford using the Superconduction Accelerator (SCA), lasing in the near infrared, and the third was at Los Alamos where lasing was observed in the mid-infrared [3].

Now, more than twenty FEL's are in use around the world, including such sites as the Institute of Nuclear Physics in Novosibirsk, Russia, Lawerence Livermore National Laboratory and the Nederlands Centrum voor Laser Research at the University of Twente.

II. BASIC FREE ELECTRON LASER THEORY

The free electron laser (FEL) is a device that transforms the kinetic energy of a relativistic electron beam into electromagnetic radiation [4]. This is accomplished by sending the electron beam through an alternating magnetic field produced by a device known as an 'undulator' or 'wiggler'. The interaction of the negatively charged electrons with the spatially periodic magnetic field induces a transverse acceleration on the electrons which causes them to give up energy to a copropagating radiation field. Adjusting certain parameters of the FEL will determine the frequency of radiation available to the resonator, where the electron beam will continue to interact with the optical field in a manner dependent on the relative phases of the electrons and the optical field. Figure 2-1 is a schematic representation of the FEL.

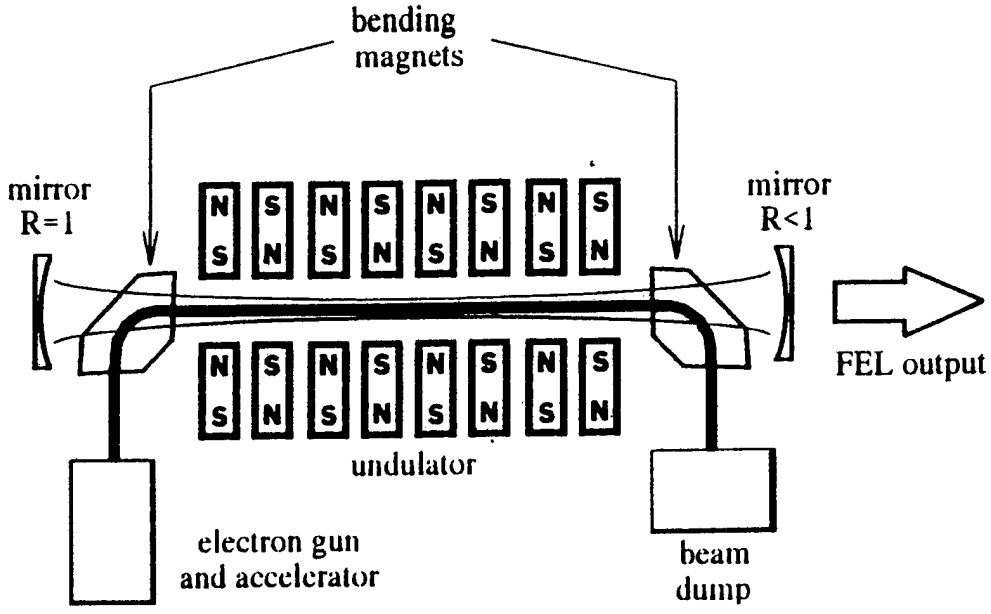

Figure 2-1. Schematic representation of the Free Electron Laser.

A. ELECTRON TRAJECTORY

The electrons entering the undulator have relativistic energy, γmc^2, where m is the electron rest mass, c is the speed of light, $\gamma = (1 - \beta^2)^{-1/2}$ is the Lorentz factor, $\beta = v/c$, and v is the electron velocity magnitude.

The motion of the electrons interacting with the undulator magnetic field and the optical field can be described by the Lorentz force equation,

$$\frac{d(\gamma\vec{\beta})}{dt} = -\frac{e}{mc}(\vec{E} + \vec{\beta} \times \vec{B}), \tag{2.1}$$

where e is the charge of an electron, $\vec{E}$ is the electric component of the optical field and $\vec{B}$ is the sum of the magnetic component of the optical field and the magnetic field of the undulator. Since the effects of the magnetic and electric components of the optical field nearly cancel, the net transverse optical force is significantly smaller than that of the undulator, so that the magnetic field in (2.1) becomes, $\vec{B} \approx B[\cos(k_o z)\hat{x} + \sin(k_o z)\hat{y}]$ for a helical undulator, where $k_o = 2\pi/\lambda_o$ is the undulator wave number, λ_o being the undulator wavelength. In a permanent magnet undulator, the undulator wavelength is dependent on magnet spacing. Substituting the equation for the magnetic field of the undulator into (2.1), and then integrating yields a helical shaped trajectory for perfectly injected electrons given by,

$$\vec{\beta}_\perp = -\frac{K}{\gamma}[\cos(k_o z)\hat{x} + \sin(k_o z)\hat{y}], \tag{2.2}$$

where $\vec{\beta}_\perp$ is the transverse component of the electron velocity and $K = e\bar{B}\lambda_o/2\pi mc^2$ is the important 'undulator parameter'. Assuming perfect injection of the electrons into the undulator cavity makes the constant of integration zero. Similar methods

can be used to describe the motion of electrons in other types of undulators, such as the planar undulator.

Other factors affect the motion of the electrons in the undulator. When viewed quantum mechanically, it is noted that a photon emitted by an electron will cause a small recoil of the electron in the opposite direction. The large energy of the relativistic electrons (50MeV) and the low energy of a photon ($\approx$ 1eV) make the quantum recoil negligible. It is for this reason that the FEL lends itself so well to classical electromagnetic theory, and can be described quite well without the use of quantum mechanics [5].

B. THE RESONANCE CONDITION

For optimum exchange of energy between an electron and the optical field, the electron must oscillate in phase with the optical field. Since the electron is moving slower than the optical field, the electron will lag behind the optical wave as they travel down the undulator. The condition for optimum energy exchange is met when the electron falls behind the optical field by the distance of one optical wavelength within the interval of one undulator wavelength.

In time Δt the optical wave will travel a distance $c\,\Delta t$ and the electron will travel a distance $\beta_z c\,\Delta t$, β_z being the axial component of the electron velocity. Taking Δt to be the time for the electron to travel one undulator wavelength we have,

$$\lambda = (c - \beta_z c)\frac{\lambda_o}{\beta_z c}, \tag{2.3}$$

where λ is the wavelength of the optical field. Noting that $\beta^2 = \beta_z^2 + \beta_\perp^2$ and using

the definition of the Lorentz factor γ in the last section,

$$\beta_z = \left[1 - \beta_\perp^2 - \frac{1}{\gamma^2}\right]^{1/2}. \tag{2.4}$$

Expanding yields,

$$\beta_z \approx 1 - \frac{1 + \gamma^2\beta_\perp^2}{2\gamma^2}. \tag{2.5}$$

Squaring (2.2) and substituting into (2.5) yields,

$$\beta_z = 1 - \frac{1 + K^2}{2\gamma^2}, \tag{2.6}$$

which when substituted into equation (2.3) gives the resonance condition,

$$\lambda \approx \lambda_o \left[\frac{1 + K^2}{2\gamma^2}\right] \tag{2.7}$$

The resonance equation reveals one of the attractive features of the FEL. Since the wavelength of the optical field can be changed by adjusting the undulator parameter and/or the energy of the electron beam, the laser is continuously tunable over a wide range of wavelengths, unlike most chemical and atomic lasers.

C. THE PENDULUM EQUATION

Having described the large-scale motion of the electron resulting from the interaction with the undulator magnetic field, the interaction of the electron with the optical field is now examined. It has been shown that electron dynamics in the FEL can be modeled well by the pendulum equation [6], which makes analysis of FEL behavior a task most personal computers can handle.

Another of the Lorentz force equations governing the FEL electron is,

$$\frac{d\gamma}{dt} = \dot{\gamma} = -\frac{e}{mc}(\vec{\beta} \cdot \vec{E}), \tag{2.8}$$

where $\vec{E} = E[\cos(kz - \omega t + \phi)\hat{x} + \sin(kz - \omega t + \phi)\hat{y}]$ is the electric component of the optical field. Substitution of (2.2) into (2.8) yields,

$$\dot{\gamma} = \frac{eKE}{\gamma mc}\cos(\zeta + \phi), \tag{2.9}$$

where $\zeta = (k + k_o)z - \omega t$ is the electron phase. Note that when $(-\pi/2 < \zeta + \phi < \pi/2)$, the cosine is positive and the electron will gain energy from the optical field. Similarly, when $(\pi/2 < \zeta + \phi < 3\pi/2)$, the cosine is negative and the electron will lose energy to the optical field.

Taking two derivatives of the electron phase ζ results in,

$$\ddot{\zeta} = (k + k_o)c\dot{\beta}_z. \tag{2.10}$$

Using $dt = Ld\tau/c$ where L is the undulator length, (2.10) can be made into the dimensionless equation,

$$\overset{\circ\circ}{\zeta} = L(k + k_o)\overset{\circ}{\beta}_z, \tag{2.11}$$

where L is the undulator length, $\overset{\circ\circ}{(\ldots)} = d^2(\ldots)/d^2\tau$ and $\overset{\circ}{(\ldots)} = d(\ldots)/d\tau$. Substituting (2.2) into (2.4) yields,

$$\beta_z^2 = 1 - \frac{1 + K^2}{\gamma^2}, \tag{2.12}$$

which when differentiated with respect to τ yields,

$$\beta_z\overset{\circ}{\beta}_z = \frac{(1 + K^2)\overset{\circ}{\gamma}}{\gamma^3}. \tag{2.13}$$

Solving for $\dot{\gamma}$ and combining with the dimensionless form of (2.9) yields,

$$\dot{\beta}_z = \frac{(1 + K^2)eKLE}{\gamma^4 mc^2 \beta_z} \cos(\zeta + \phi). \tag{2.14}$$

Substituting this into (2.11), assuming $k \gg k_o$, noting that $\beta_z \approx 1$, and imposing the resonance condition $\lambda = \lambda_o (1 + K^2)/2\gamma^2$ gives the pendulum equation,

$$\ddot{\zeta} = \frac{4\pi NeKLE}{\gamma^2 mc^2} \cos(\zeta + \phi) = |a| \cos(\zeta + \phi), \tag{2.15}$$

where $|a| = 4\pi NeKLE/\gamma^2 mc^2$ is the dimensionless optical field strength.

D. THE OPTICAL WAVE EQUATION

The optical wave equation couples the electrons to the copropagating optical wave by relating the electron phase to the change in the optical field. The relative phase between electron oscillation and the driving force determines whether stimulated emission (energy transferred to the optical field) or absorption from the field will occur [7].

The optical wave equation is,

$$\left[\vec{\nabla}^2 - \frac{1}{c^2}\frac{\partial^2}{\partial t^2}\right]\vec{A}(\vec{x},t) \approx -\frac{4\pi}{c}\vec{J}_\perp(\vec{x},t), \tag{2.16}$$

where $\vec{A}(\vec{x},t) = [E(z,t)/k](\sin\Psi\hat{x} + \cos\Psi\hat{y})$, $\Psi = (kz - \omega t + \phi)$ and $\vec{J}_\perp$ is the transverse electron beam current. An approximation for the amplitude and phase is made in which the field is assumed to vary slowly over the space and time of one optical wavelength and one optical period. This means that $\dot{E} \ll \omega E$ and $\dot{\phi} \ll \omega\phi$.

Substituting the vector potential $\vec{A}$ into (2.16) and dropping all terms containing two derivatives yields,

$$\frac{\partial E}{\partial t} = -2\vec{J}_{\perp} \cdot \hat{\varepsilon}_1, \tag{2.17}$$

and

$$E\frac{\partial \phi}{\partial t} = 2\pi\vec{J}_{\perp} \cdot \hat{\varepsilon}_2, \tag{2.18}$$

where $\hat{\varepsilon}_1$ and $\hat{\varepsilon}_2$ are the orthogonal unit vectors $(\cos\psi\hat{x} - \sin\psi\hat{y})$ and $(\sin\psi\hat{x} + \cos\psi\hat{y})$, respectively.

Each electron in the beam contributes to the transverse electron beam current such that,

$$\vec{J}_{\perp} = \sum_i \vec{J}_{\perp i} = \sum_i -ec\,\vec{\beta}_{\perp}\delta^{(3)}(\vec{x} - \vec{r}_i), \tag{2.19}$$

where $\vec{r}_i$ is the position of the i^{th} electron and $\delta^{(3)}$ is the three dimensional Dirac delta-function. Using (2.2) for $\vec{\beta}_{\perp}$, substituting (2.19) into (2.17) and (2.18), performing the dot products and assuming a constant electron density ρ while summing over all sample electrons yields,

$$\dot{E} = \frac{-2\pi eKc}{\gamma}\rho\langle\cos(\zeta + \phi)\rangle, \tag{2.20}$$

and

$$E\dot{\phi} = \frac{2\pi eKc}{\gamma}\rho\langle\sin(\zeta + \phi)\rangle, \tag{2.21}$$

where $\rho\langle\ldots\rangle$ replaces the summation over all electrons by a weighted average of sampled electrons at a specific site, the electrons within one optical wavelength. This substitution is possible due to the slowly varying approximation discussed above. Use is also made of the previous definition, $\zeta = (k + k_o)z - \omega t$.

Using the dimensionless beam current $j = 8N(e\pi KL)^2\rho/\gamma^3 mc^2$, and the previous definition for $|a|$, then (2.20) and (2.21) will yield

$$\dot{|a|} = -j\langle\cos(\zeta + \phi)\rangle \,,\; \dot{\phi} = \frac{j}{|a|}\langle\sin(\zeta + \phi)\rangle, \tag{2.22}$$

or,

$$\dot{a} = -j\langle e^{-i\zeta}\rangle, \tag{2.23}$$

where $a = |a|e^{i\phi}$ is the complex dimensionless optical field. Note that when $(\zeta + \phi) \approx \pi$, the optical field will grow. Conversely, when $(\zeta + \phi) \approx \pi/2$, there is a decrease of the optical field. Note also that an increase in the optical field strength will result in a decrease in the optical phase evolution, while an increase in the dimensionless electron beam current will have the opposite effect.

E. PHASE SPACE PLOTS

The evolution of an individual electron can be described by the pendulum equation (2.15) and the optical wave evolution can be described by the wave equation (2.23). Together these equations describe the FEL interaction through the dimensionless current density j, since j determines the response of the optical wave to the bunching of the electrons in phase space. The bunched electrons radiate coherently to contribute to the optical field, but only a small increase in the optical power at the resonant wavelength is obtained on each pass. Due to the collecting nature of the resonator, substantial amplification of the optical wave is achieved after many passes.

Another important parameter of the electrons is the electron phase-velocity, $\nu = \dot{\zeta} = L[(k + k_o)\beta_z - k]$. Phase-space plots showing the evolution of ν and ζ for

an electron over one pass in the undulator are useful in understanding the FEL interaction. In the low gain FEL, the equation,

$$\nu^2 = \nu_o^2 - 2|a|[\sin(\zeta + \phi) - \sin(\zeta_o)], \tag{2.24}$$

describes the phase-space paths followed by electrons, where $\nu_o = \nu(0)$ and $\zeta_o = \zeta(0)$ are the initial conditions in phase space of the electrons. In the coordinates (ζ,ν), a pendulum has a stable fixed-point at $(\pi/2,0)$ and an unstable fixed point at $(3\pi/2,0)$. Closed and open paths will be determined by which of these points the electron is orbiting in phase space. A curve can be superimposed in phase space which will differentiate closed and open space orbits. This curve is known as the 'separatrix' and has the form,

$$\nu_s^2 = 2|a|[1 - \sin(\zeta_s + \phi)]. \tag{2.25}$$

Notice that the peak-to-peak height of the separatrix is $4|a|^{1/2}$ and the horizontal position is determined by ϕ.

Figure 2-2 is a phase space plot of the final positions at $\tau = 1$ of 40 sample electrons with $j = 1$. The separatrix is plotted inside the phase space area for reference. The electrons enter the undulator with an initial uniform spread in phase between $\zeta = -\pi/2$ to $\zeta = 3\pi/2$ with initial phase-velocity $\nu_o = 2.6$, and interact with an initial optical field of $a_o = 4$. The electrons located in the region $\zeta = \pi/2$ to $\zeta = 3\pi/2$ will loose energy and move down in ν according to (2.15). With this bunching of electrons near $\zeta = \pi$, there will be net gain in the FEL and the optical field will grow through (2.23). The equation for gain is,

$$G(\tau) = \frac{[a(\tau)^2 - a_o^2]}{a_o^2}, \tag{2.26}$$

gain being the fractional increase in power per unit time. Gain is shown in the upper right of the figure, below which the corresponding optical phase shift is plotted. The gain takes some time to increase due to the initial uniform distribution of the electrons.

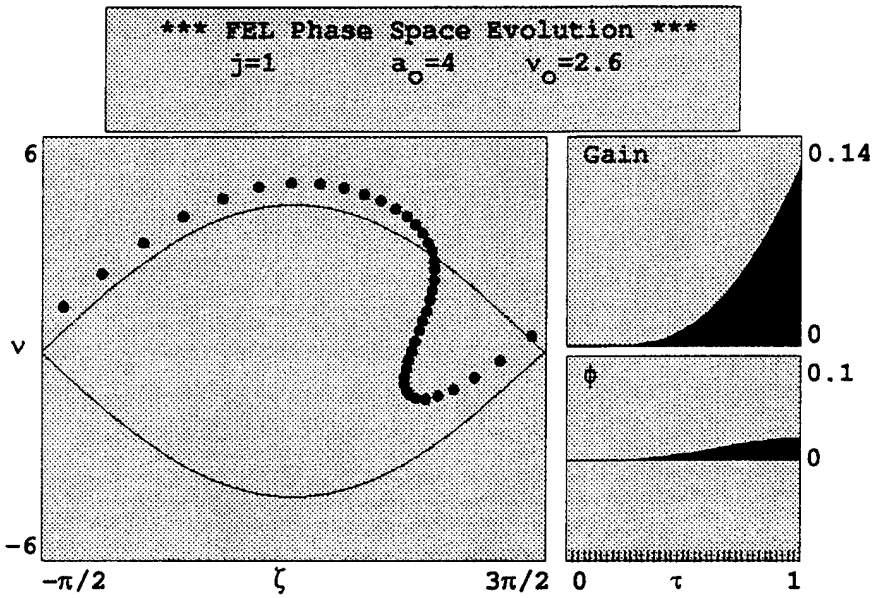

Figure 2-2. Phase space plot for a low gain FEL. Electron bunching is occurring near $\zeta = \pi$.

With an expansion of the pendulum equation (2.23) for weak fields $a_o \ll \pi$, an analytical expression for the gain can be obtained [7]. If we assume that the electrons are initially uniformly distributed in phase ζ_o and monoenergetic with phase-velocity ν_o, then the average energy lost by an electron is $\gamma mc^2(\langle\nu\rangle - \nu_o)/4\pi N$. With a loss in electron energy, there is gain in the FEL. This allows a contribution from the second-order term of the pendulum equation expansion to the gain $G(\tau) = 2j(\nu_o - \langle\nu\rangle)/a_o^2$. Thus, the gain develops along the undulator as,

$$G(\tau) = j\left[\frac{2 - 2\cos(\nu_o\tau) - \nu_o\tau\sin(\nu_o\tau)}{\nu_o^3}\right]. \tag{2.27}$$

Figure 2-3 is a sample gain spectrum plot. The gain spectrum is anti-symmetric about ν_o and has a peak gain of $G = 0.135j$ at $\nu_0 = 2.6$. Note that electrons with positive phase velocities near resonance will amplify the optical wave and electrons with negative phase velocities near resonance will absorb energy from the optical wave. Phase velocities far off resonance, $|\nu_o| \gg \pi$ will produce small oscillations shifting between amplification and absorption.

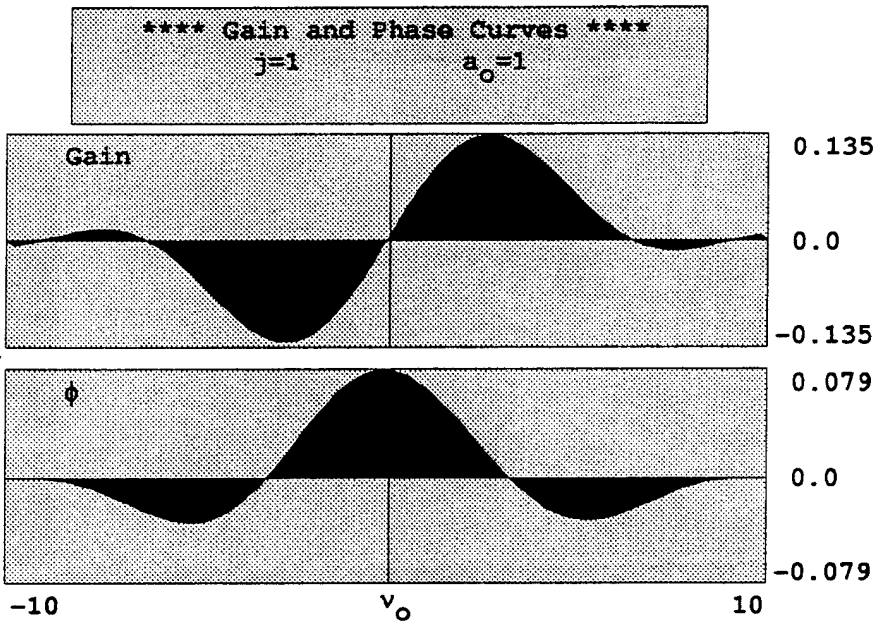

Figure 2-3. Gain curve for a low current, low gain FEL. Curve is anti-symmetric about ν_o.

The natural gain bandwidth is $\Delta\nu_o \approx \pi$ about the point $\nu_o = 2.6$. Since a change in the electron energy $\Delta\gamma mc^2$ is equivalent to a change in phase-velocity $\Delta\nu = 4\pi N\Delta\gamma/\gamma$ the FEL natural gain bandwidth becomes,

$$\left|\frac{\Delta\gamma}{\gamma}\right| \approx \frac{1}{4N}. \tag{2.28}$$

A change in the electron beam energy (with a corresponding change in resonance) will act to shift the gain curve along the ν_o axis. With a change in electron beam energy $\Delta\gamma \approx \gamma\Delta\nu_o/4\pi N$ the ν_o axis will become a function of the resonant energy $\gamma \approx [\lambda_o(1 + K^2)/2\lambda]^{1/2}$.

In strong optical fields, the gain spectrum distorts. Strong optical fields begin when $|a| \gtrsim \pi$. More of the electron energy will be transferred to the optical field (due to increased bunching), but the gain will decrease due to the onset of saturation. Saturation occurs when the electron bunch moves past $\zeta \approx \pi$ where electrons give up energy to the optical field.

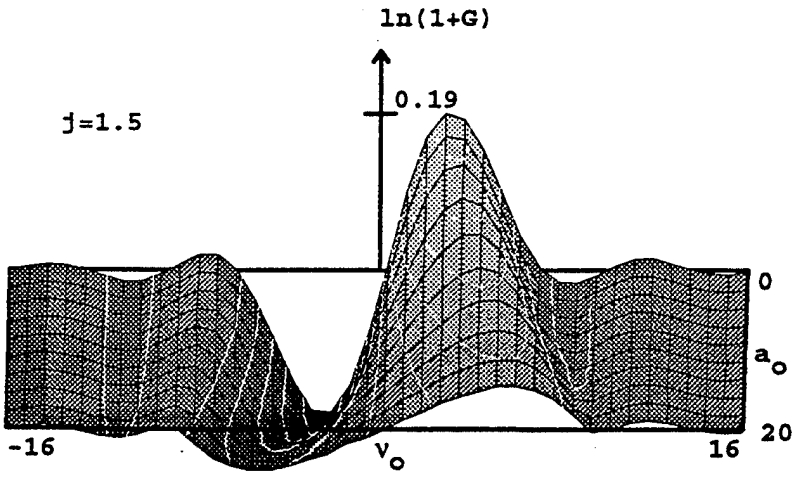

Figure 2-4. Low current gain spectrum $G(\nu)$ as a function of increasing optical field strength a_o.

When overbunching occurs, the electrons absorb energy from the optical field, and gain begins to fall off. Figure 2-4 shows the relationship between the gain spectrum and the optical field a_o. As a_o increases, three things occur. The peak gain decreases, as discussed above, the gain spectrum widens, and the value of, ν_o giving peak gain, shifts to the right. The width of the gain curve is given by $\Delta\nu_o \approx 2|a|^{1/2}$, so more frequencies will experience gain, but at a lower gain value than if a_o were lower. For $a_o = 20$, it can be seen that peak gain occurs at $\nu_o \approx 5$.

F. MODE COMPETITION

In the low current, low gain FEL, modes within the oscillator evolve independently [7]. We can observe the development of a mode since we have the expression for the weak-field gain in a single pass, and this can be applied to multiple passes. In a low gain FEL, mode competition will be observed over many passes. This will have the effect of narrowing the frequency spectrum and increasing the coherence length of the optical wave. Using (2.27) we can analyze multiple modes over many passes simultaneously.

In the longitudinal dimension, the modes are scaled by the gain bandwidth (2.28) and normalized to the slippage distance $N\lambda$. This is the distance that the resonant electron will lag the optical pulse at the end of the undulator. At resonance, exactly one wavelength of light will pass over an electron as the electron passes through the undulator [7]. Thus, the interaction distance for the optical wave and the electron is the slippage distance and the initial coherence length will be $N\lambda$. In the transverse direction, modes are scaled by the factor $(L\lambda/\pi)^{1/2}$, which is the approximate radius of the optical beam. With a relativistic electron beam,

the intermode spacing becomes $\Delta\nu(k) \approx \gamma^{-2}$ which is small compared to the size of the mode. We can then say that the FEL has a continuum of modes across a gain spectrum bandwidth of $\Delta\nu \approx \pi$.

The phase-velocity,

$$\nu(k) = L[(k + k_o)\beta_z - k], \tag{2.29}$$

identifies each longitudinal mode or wavelength $\lambda = 2\pi/k$. On each pass the optical power in each mode is increased from spontaneous emission, and the gain spectrum. The contribution from spontaneous emission is $s(\nu) \propto [\sin(\nu/2)/(\nu/2)]^2$, which is symmetrical in shape and has width $\Delta\nu \approx 2\pi$. The equation for the change in optical power on successive passes is given by

$$\Delta P_n(\nu) = s(\nu) + P_n(\nu)[G(\nu) - 1/Q], \tag{2.30}$$

where $P_n(\nu)$ is the optical power in mode $\nu(k)$, and $s(\nu)$ is the spontaneous emission into mode $\nu(k)$ on each pass. The factor Q is a measure of the optical losses at the resonator mirrors. The quantity $e^{-n/Q}$ describes the optical loss per mode over n passes in the resonator and is independent of ν.

G. LONGITUDINAL MULTIMODE THEORY

In radio-frequency accelerators (such as the one used by the Stanford Free Electron Laser Facility) short picosecond electron pulses are produced by the accelerating microwave field. These short pulses require a more complete approach to describe the optical field coupling to the electron beam [7].

As each micropulse enters the undulator, a short optical pulse is formed by spontaneous emission which begins to travel back and forth between the mirrors of

the resonator. In order for light amplification to occur, the light pulse must arrive at the beginning of the undulator at the same time as the next electron pulse. Because the electron pulse is traveling slower than the light pulse, it will lag the light pulse as it travels towards the end of the undulator. Taking the length of the undulator to be L, the interaction time between optical pulse and electron pulse will be L/c. This creates a slippage difference $N\lambda \approx (c - c\bar{\beta}_z)(L/c)$, where $\bar{\beta}_z$ is the speed of the electron pulse. Short pulse effects must be taken into account when the electron pulse length approaches the slippage distance $N\lambda$.

Normalization of longitudinal distances to this slippage distance is made such that $z/N\lambda \rightarrow z$. Multiple sites along the complex wave envelope are tracked so that $a \rightarrow a(z)$ which is equivalent to an extension of longitudinal wavenumbers $a \rightarrow a(k)$. Therefore, the pendulum equation (2.15) becomes,

$$\overset{\circ\circ}{\zeta}_{z-\tau} = |a_z| \cos(\zeta_{z-\tau} + \phi_z), \tag{2.31}$$

and the optical wave equation (2.23) becomes,

$$\overset{\circ}{a}_z = -j_{z-\tau} \langle e^{-i\zeta_{z-\tau}} \rangle, \tag{2.32}$$

where z refers to a particular optical site along the undulator and $z-\tau$ is an electron site which has slipped along the optical pulse in time τ due to the electrons' slower velocity. As the electrons move back along the optical pulse they transfer information from one optical site to another. In effect, the light traveling at speed c remains fixed in z while the electrons move back to site $z-\tau$ interacting along the way with sites in the optical wave envelope. The dimensionless current density becomes $j(z) = 8N(\pi eKL)^2 \rho(z)/\gamma^3 mc^2$, where $\rho(z)$ is the electron particle density at site z. The electron pulse shape is taken to be parabolic and of the

form,

$$j = \begin{cases} j_o(1 - 2z^2/\sigma_z^2) & \text{for} \quad j(z) > 0 \\ 0 & \text{for} \quad j(z) = 0, \end{cases} \tag{2.33}$$

where j_o is the peak beam current and $\sigma_z = l_e/N\lambda$ normalizes the electron pulse length l_e.

The number of sites to be examined is defined as N_W which varies depending on the amount of detail needed for a particular pulse length. W is the width of the window being examined and is an integral number of slippage distances long as given by $W = N_W \Delta z$, where Δz is the dimensionless spacing between sites. In this way the modes represented in the window are given by,

$$\nu_l = \nu_o \left[\frac{\pi}{W}\right](2l - N_W) \quad \text{where} \quad l = 0,1,2,3,...,N_W - 1, \tag{2.34}$$

where l is an integer and the spacing between optical modes is $\Delta\nu = 2\pi/W$. We can set the site spacing Δz equal to the integration time step $\Delta\tau$ so that the electrons slip back one site for each time step.

H. TRAPPED-PARTICLE INSTABILITY

The effects of trapped-particle instability can be studied causes the FEL to evolve from a single mode to a few modes [7]. Once the optical field has grown large, the FEL interaction can cause overbunching of the electrons in phase space. Deep potential wells caused by the optical field will act to trap the electrons, which can drive the carrier wave unstable and cause sideband frequencies to grow from noise [7].

The pendulum equation (2.15) can be expanded about the stable fixed point $\zeta = \pi/2$, so that $\zeta = \pi/2 + x$ where $x \ll \pi$. A solution describing the motion of a trapped electron is,

$$\zeta(\tau) \approx \zeta_o + \frac{\nu_o}{\nu_s}\sin(\nu_s \tau), \tag{2.35}$$

where $\nu_s = |a|^{1/2}$ is the 'synchrotron' or trapped-particle frequency. This will produce sidebands in the optical power with frequency $\nu = \nu_o \pm \nu_s$ and wavelengths shifted from the fundamental by $\Delta\lambda/\lambda = \nu_s/2\pi N$. This effect will change a coherent single frequency mode into a mode with two sidebands.

The onset of trapped-particle instability can be seen in Figure 2-2. For a full synchrotron oscillation, the optical field strength would have to be $|a| = 4\pi^2 \approx 40$, which corresponds to a separatrix height of $4|a|^{1/2} \approx 25$. This would cause the electrons to travel in a closed orbit about the fixed point $(\zeta,\nu) = (\pi/2,0)$ in phase space. In the figure, the height of the separatrix is $4|a|^{1/2} = 8$, and isn't sufficient to cause a full cycle of synchrotron oscillation. If the optical field were stronger, overbunching would occur as the electrons were trapped in the potential well caused by the strong optical field, and the gain would fall towards zero as the oscillating optical field degraded the gain mechanism. Since the parameters j and Q determine the optical field strength, changing these will determine the onset of trapped particle instability. Also a factor in short-pulse FEL's is desynchronism, discussed below.

I. DESYNCHRONISM

When each electron pulse from the accelerator and the rebounding optical pulse stored in the resonator always start together at one end of the undulator, they are synchronized and the dimensionless desynchronism factor $d = 0$. While passing through the undulator, the faster moving optical pulse moves ahead of the electron pulse. In Figure 2-5 the position of the electron pulse relative to the optical field $|a(z,n)|$ can be seen in the left-most portion.

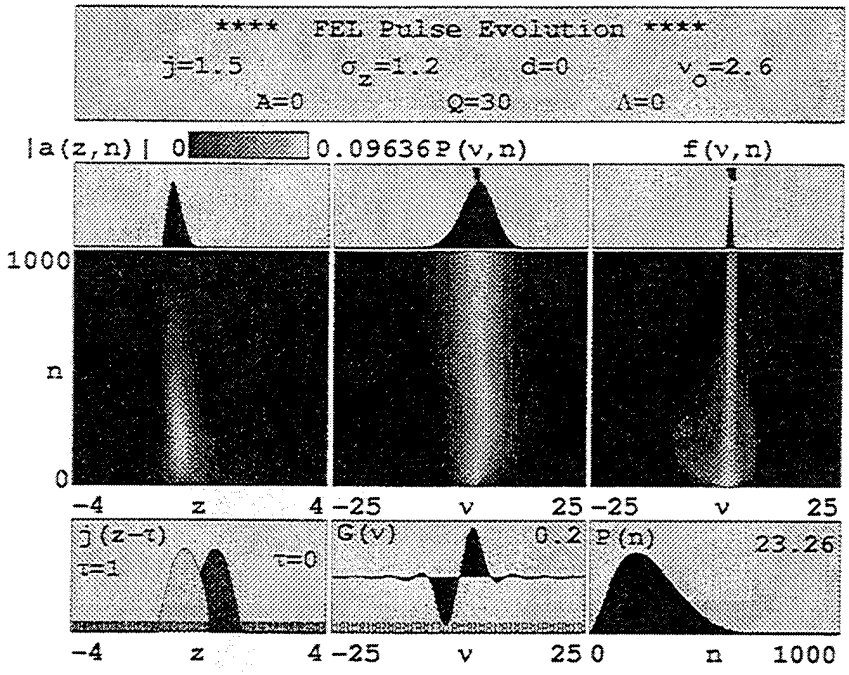

Figure 2-5. FEL pulse evolution. Optical field $|a(z,n)|$ and output power $P(n)$ grow initially, but die out with $d = 0$.

The optical field is center left and directly above the electron pulse diagram. At the top left is the final optical pulse shape and above is the scale for the optical field plot. The electron pulse has a dimensionless length of $\sigma_z = 1.2$. The darker electron envelope represents the electron pulse at $\tau = 0$ and the lighter envelope is

lagging the optical pulse upon reaching the end of the undulator.

In the center of the figure, the optical power spectrum evolution $P(\nu,n)$ is plotted with the final optical power spectrum directly above it. To the right of the optical power is the electron phase-velocity spectrum evolution $f(\nu,n)$ with the final electron phase-velocity spectrum directly above it. In the optical power evolution plot, the triangular tic mark denotes the initial position of the central wavelength at resonance. As the FEL gain mechanism takes effect, the anti-symmetric shape of the gain curve shifts the resonant wavelength to the right towards $\nu_o \approx 2.6$ with a corresponding shift in the optical power spectrum. Initially, the electrons move back and forth on the phase-velocity plot $f(\nu,n)$, moving farther to the left than to the right. This indicates a net contribution of energy to the optical wave as shown by the growing optical pulse on the far left.

By the time the electrons have bunched and increased the FEL gain, the electron pulse is contributing energy preferentially to the tail end of the slower moving optical pulse. This can be seen in the figure by noting that the optical pulse is above the lighter electron pulse envelope and moves to the left with increasing n. After $n \approx 500$ passes, the electron phase-velocity spectrum $f(\nu,n)$ has narrowed considerably, with the corresponding effect that significant energy is no longer being transferred to the optical wave. The optical field has all but died out, and the optical power $P(n)$ shown in lower right is near zero. By the end of the run, the power has reached zero since the optical pulse has moved too far ahead of the electron pulse, and the optical power spectrum has widened with the effect of narrowing the optical field $|a(z,n)|$. At exact desynchronism $d = 0$, the

FEL does not operate.

Figure 2-6 shows short pulse evolution with $d = 0.02$. The optical power spectrum $P(\nu,n)$ once again shifts to the right, but narrows to a stable resonance wavelength after about $n = 250$ passes. The electron phase velocity spectrum reaches a stable position to the left of $\nu_o = 0$ so that electrons now continue to contribute energy to the optical phase in a steady-state manner.

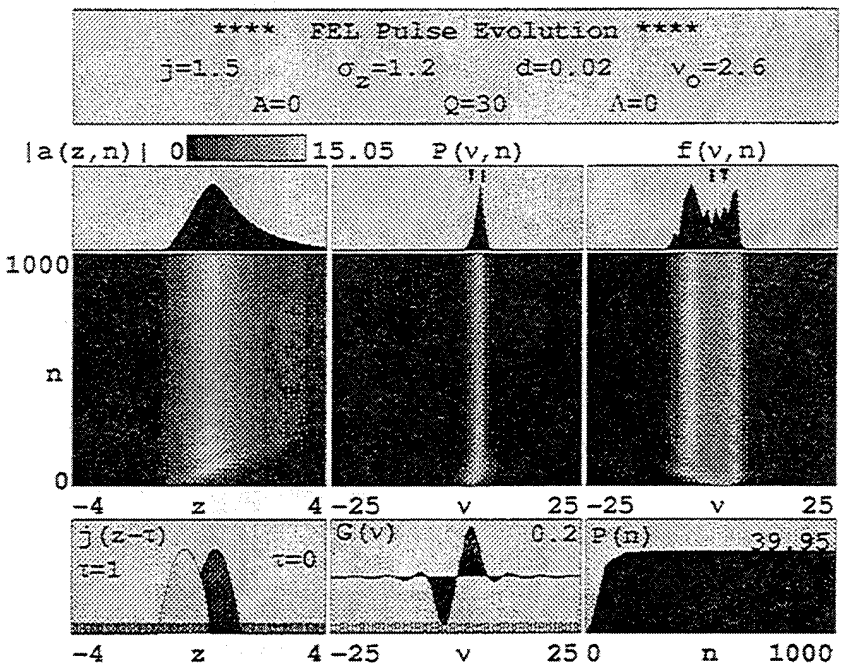

Figure 2-6. With $d = 0.02$, the optical field and output power grow to steady state.

Since the electrons now have a longer interaction time with the optical wave, the optical wave has lengthened. The centroid of the optical field is above the center position of the electron pulse between $\tau = 0$ and $\tau = 1$ indicating that the electrons are contributing more towards the center of the optical pulse and not the tail, as before.The optical field has stabilized and the FEL reaches steady state at about $P(n) \approx 41$. When short-pulse gain is above the coupling threshold for the FEL,

desynchronism is very important to pulse evolution and final saturation [7].

J. LIMIT-CYCLE BEHAVIOR

Short-pulse theory predicts a phenomenon known as limit-cycle behavior which affects the optical pulse structure and power [7]. As electrons moves back along the optical pulse, they continue to radiate coherently, forming an optical subpulse at the tail of the optical pulse. The amplification is at the rear of the optical pulse because the electrons don't bunch enough for gain until they are near the end of the optical pulse. In effect, the optical pulse centroid is moving with a speed slightly less than c. Desynchronism is used to move the centroid of the optical pulse back towards the center, but as it does so, the optical wave can

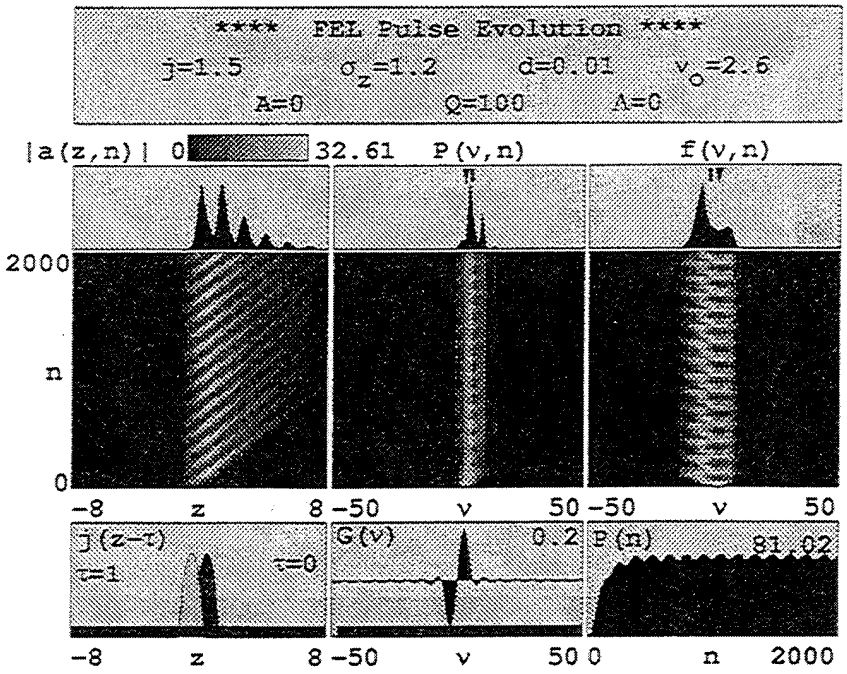

Figure 2-7. Limit-cycle behavior. Subpulses move through the optical pulse $|a(z,n)|$, causing the output power $P(n)$ to modulate.

fluctuate due to the subpulses moving through it. The optical field envelope $|a(z,n)|$ in Figure 2-7 shows the limit-cycle behavior in a short pulse FEL with $\sigma_z = 1.2$. The beam current is $j = 1.5$, and $Q = 100$.

Sidebands have developed in the optical power $P(\nu,n)$ which initiated after a small number of passes and stablized over many passes. The spacing of the sidebands is given by $\nu_s \approx \sqrt{a} \approx \sqrt{30} \approx 5.5$. The power $P(n)$ shows the periodic modulation due to the shifting nature of the optical field, and has settled into a stable modulation at $P(n) \approx 81$. The multiple frequencies have given rise to a modulated optical field envelope $|a(z,n)|$. As d is increased, the limit-cycle behavior disappears. At around $d = 0.028$ the weak field gain is at a maximum, and the effects of trapped-particles is diminished. As in the trapped-particle instability, changing the parameters Q, d and j will affect whether or not limit-cycle behavior will be evident.

III. RESONANT WAVELENGTH MODULATION

A. SIMULATING ELECTRON BEAM ENERGY MODULATION

A two dimensional simulation in z and t is used to examine the effects of electron beam energy modulation on optical power and phase evolution in a short pulse FEL. Modulation of the electron beam energy in a free electron laser is equivalent to a modulation of the resonant wavelength. A two dimensional simulation is used to study modulations of various frequencies and amplitudes. Parameters were chosen to represent the Stanford University Super Conducting Accelerator (SCA) FEL where the effects have been studied experimentally [8].

As stated earlier, the change in resonance due to a variation in the electron beam energy $\Delta\gamma mc^2$ is given by $\Delta\nu = 4\pi N\Delta\gamma/\gamma$ where ν is the dimensionless electron phase-velocity and N is the number of periods in the undulator [7]. Over many passes, the beam energy modulations are simulated by superimposing a sinusoidal variation in electron phase-velocity around ν_o. The resonant phase-velocity becomes,

$$\nu(n) = \nu_o + A\sin[2\pi n/\Lambda]. \tag{3.1}$$

The electron beam phase-velocity is modulated by amplitude A and makes one complete oscillation after Λ passes through the oscillator. Low values of modulation are studied near $A = 0.1\pi$. The periods of modulation studied are in the range $\Lambda = 4000 \rightarrow 25$. The time for one pass in the FEL is $\Delta t = 2S/c$ and the frequency is thus $f = c/(2S\Lambda)$. Using the Stanford FEL parameters, each pass is $\Delta t \approx 85$ nanoseconds in length, so that the range of frequencies studied is $f \approx 3$ kHz $\rightarrow$ 470 kHz.

B. SMALL AMPLITUDE ELECTRON BEAM ENERGY MODULATION

Figure 3-1 shows the effect of a moderate electron energy beam modulation on a short pulse FEL over n = 2000 passes. The period of modulation is Λ = 1500

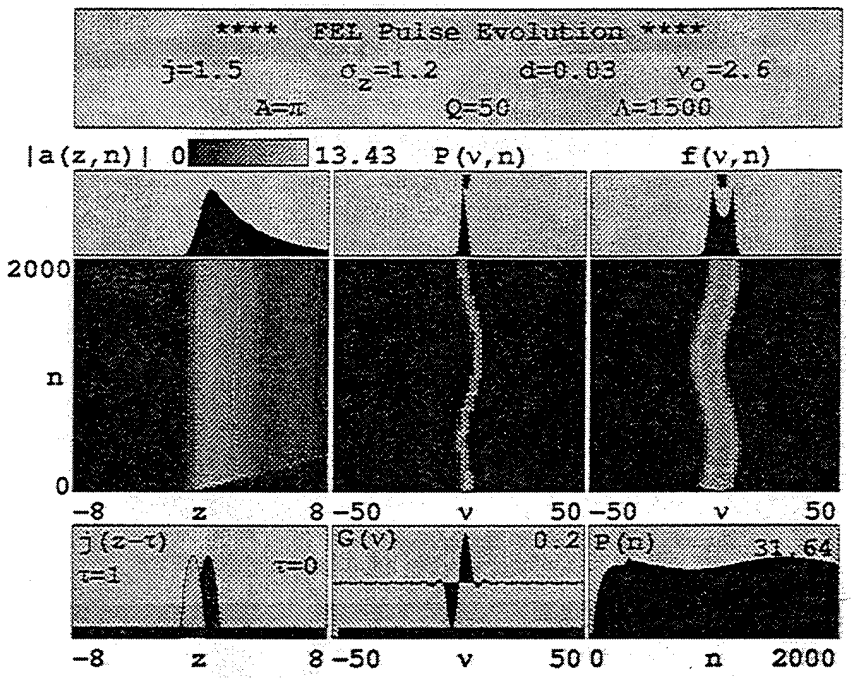

Figure 3-1. FEL pulse evolution with small amplitude electron energy beam modulation. Optical power $P(\nu,n)$ follows modulations, as does output power $P(n)$.

passes and the modulation amplitude is $A = \pi$ with beam current j = 1.5. The loss factor is Q = 50 and desynchronism is d = 0.03. One period of oscillation can be seen in the optical power evolution $P(\nu,n)$, which remains narrow due to mode competition. The electron phase-velocity $f(\nu,n)$ oscillates in the opposite direction of the optical power. The electron phase-velocity $f(\nu,n)$ oscillates as the resonant phase-velocity is modulated, as indicated in (3.1). As $f(\nu,n)$ slews to the right, indicating a bunching of electrons to the above $\nu = 0$ and a net decrease from the optical field, a minimum forms in the optical field, as denoted by a decrease in the lighter portions of the optical field plot, $|a(z,n)|$. This results in a decrease in optical power $P(\nu,n)$, and the optical power evolution slews to the left, indicating

the optical power frequency has moved below $\nu = 0$. In the same manner, as the resonant electron phase-velocity slews to the left, indicating a bunching of electrons below $\nu = 0$, energy is added to the optical field, as denoted by a widening of the lighter regions in the plot of $|a(z,n)|$.

The two peaks in the final envelope of $f(\nu,n)$ correspond to the points in ν-space where electrons collect at the end of each pass in the undulator. The peak on the right corresponds to electrons on phase-space paths near the top of the separatrix, while the left peak corresponds to electrons on phase-space paths at the bottom of the separatrix. Moving from the right to the left along the ν axis corresponds to vertical movement on the phase space plot (Figure 2-1) described earlier, and a corresponding contribution to the optical wave. The output power optical

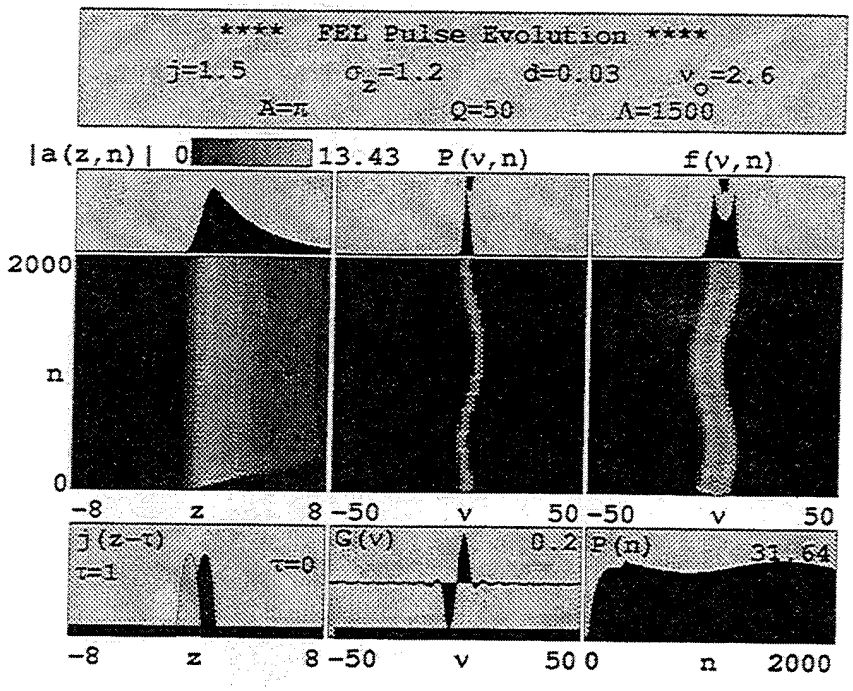

Figure 3-2. Frequency of electron beam energy modulation is increased. The FEL still follows the modulations.

power $P(n)$ oscillates with the same frequency and amplitude as the electron beam energy modulation and peaks at $P(n) \approx 32$. The optical field envelope is smooth and has a peaks of $|a(z,n)| \approx 13$. In figure 3-2 the period of modulation has been reduced to $\Lambda = 500$, and all other parameters are the same as in the previous figure. The maximums in the optical field now become more pronounced and correspond to a slew to the left of the electron phase velocity as the resonant frequency decreases, and the electrons contribute to the optical field.

With an decrease in the loss factor Q, the losses on each pass will be greater, so the peak power $P(n)$ will be correspondingly less, as shown in Figure 3-3, where the peak power is $P(n) \approx 19$. The optical field envelope has become shorter due to the increased losses of the higher longitudinal modes in the optical pulse. Otherwise, no significant differences are evident from the higher Q value.

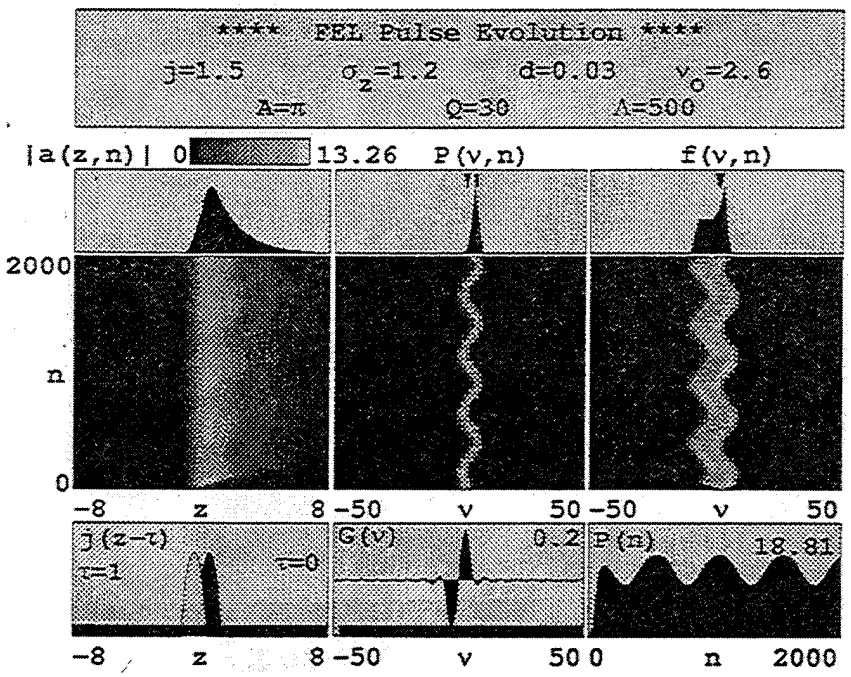

Figure 3-3. A decrease in Q decreases the width of the optical pulse and lowers the output power $P(n)$.

Figure 3-4 is made with a higher Q factor than the previous two figures, with $Q = 100$ now. The loss on each pass in the resonator in this case are small, and

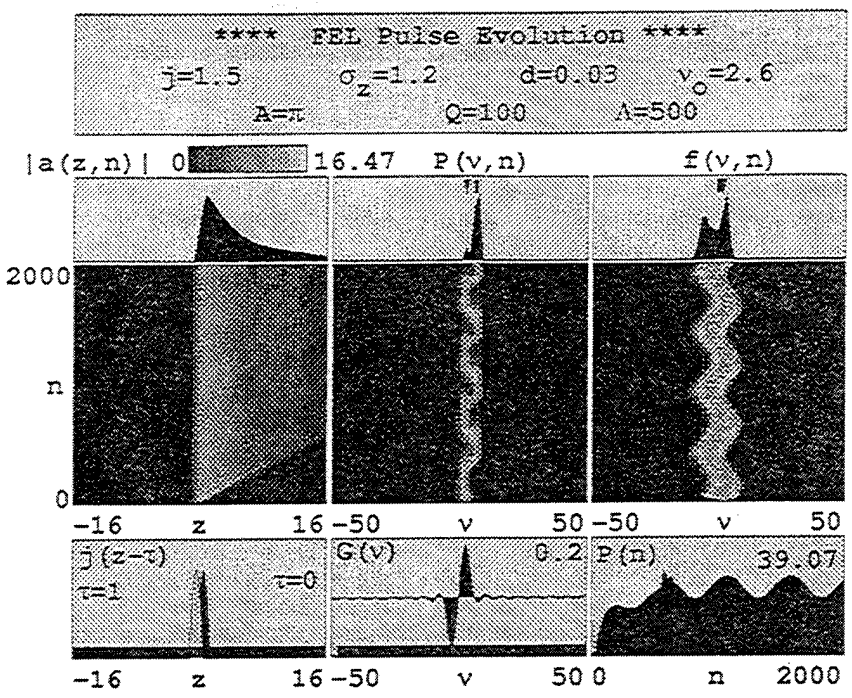

Figure 3-4. An increase in Q increases the width of the optical pulse, raises the output power $P(n)$, and begins to keep the optical power $P(\nu,n)$ from following the electron beam energy modulations.

the FEL takes more passes to stabilize the modulations. $P(n)$ initially levels out after about $n = 150$, resisting the changes in the electron beam energy modulation. Then as the losses finally diminish the older modes, $P(n)$ settles into steady oscillation after about $n = 300$ passes with a peak power $P(n) = 158$. With less loss in the resonator, the FEL 'remembers' older modes and resists movement of the resonant wavelength. For this reason, the optical field $|a(z,n)|$ retains modes farther along the z axis. The turning points in the optical power evolution are beginning to show signs of modulation resistance as well. Instead of a clean turn from the peaks of the maximum and minimum resonant frequencies, the optical power tends to continue along vertical lines at the min and max frequencies, even after some of the modes have started to slew towards the center of the optical

power spectrum.

Using the same parameters from Figure 3-2, Figure 3-5 is the short pulse evolution with altered value $d = 0.02$. With a decreased desynchronism, the optical field envelope has narrowed since the electron-optical interaction occurs over a shorter space and not as much information is transferred to the optical pulse. The optical field peaks at a higher value of $|a(z,n)| \approx 19$ with a corresponding increase in peak power $P(n) \approx 40$ compared to $|a(z,n)| \approx 15$ and $P(n) \approx 34$ for $d = 0.03$ in Figure 3-2.

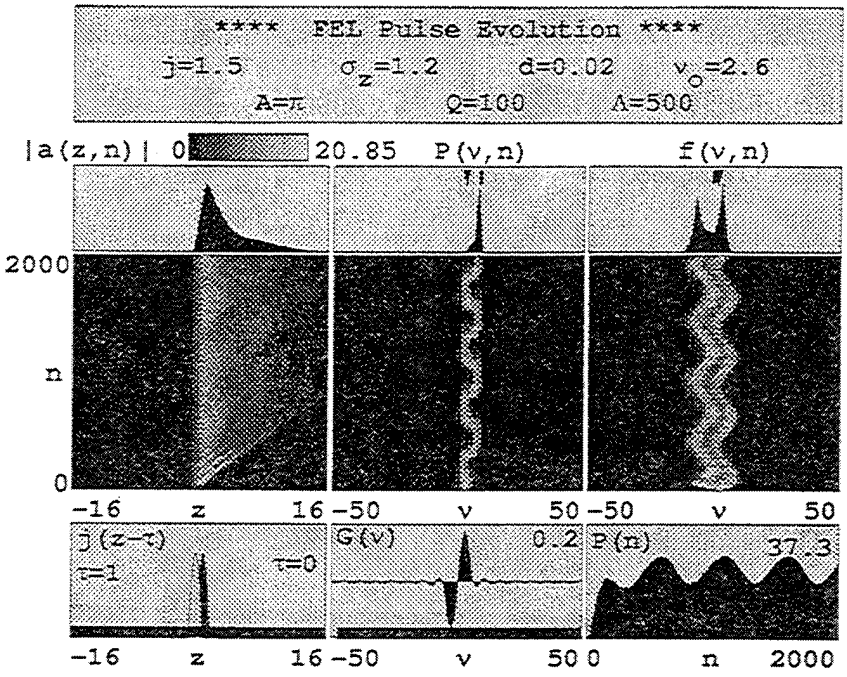

Figure 3-5. Decreasing d decreases the optical pulse width and increases output power $P(n)$.

In Figure 3-6, the desynchronism has been increased to $d = 0.05$. The characteristic lengthening of the optical pulse is evident with corresponding drop in optical field peak values. The peak power is lower than that of Figure 3-3, where the same loss factor Q and period of oscillation Λ were used.

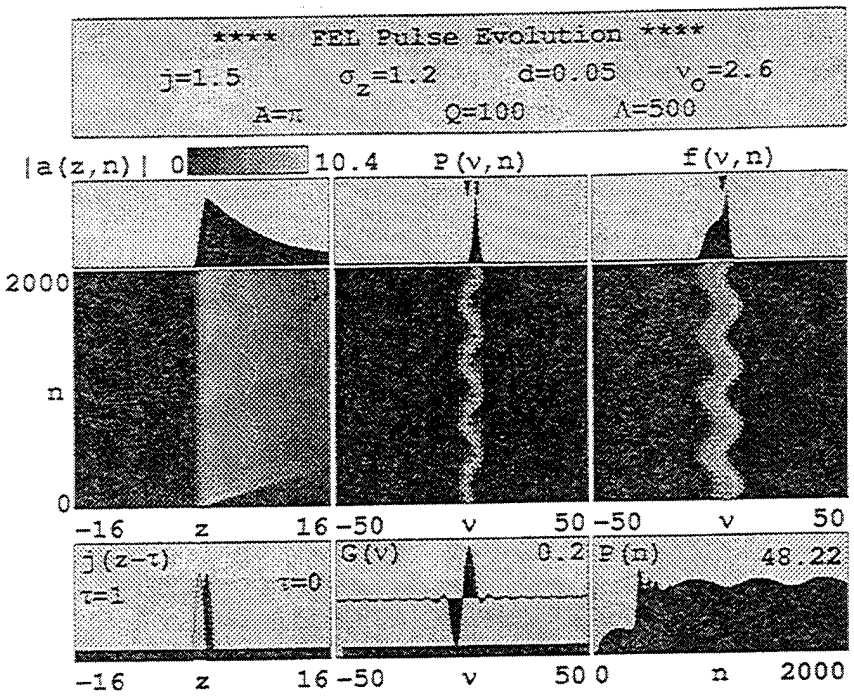

Figure 3-6. Decreasing d decreases the optical pulse width and increases output power $P(n)$.

C. OPTICAL PHASE PROGRESSION

The optical phase progression along the optical pulse $\phi(z)$ shows how the electron beam energy modulation changes the resulting optical wavelength. Since short electron pulses are used, short optical pulses described by $a = |a|e^{i\phi}$ are formed within the resonator, where ϕ is the optical phase. The magnitude of the optical field is $|a| = 4\pi NeKLE/\gamma^2 mc^2$ whose evolution, along with the optical phase evolution, can be described by (2.22). Recalling the vector potential presented earlier, an expression for the optical field vector potential can be derived, $A_{op} \propto \exp(ikz - i\omega t + i\phi)$. At any fixed time, say $t = 0$, the change in vector potential magnitude with respect to a longitudinal distance z can be expressed,

$$\frac{dA_{op}}{dz} = i(k + d\phi/dz)A_{op} = ik'A_{op}, \tag{3.2}$$

where the modified wavenumber is identified as $k' = (k + d\phi/dz)$. Substitution of (3.2) into (2.29) and noting that $\lambda_o \approx \lambda(1 - \beta_z)$ near resonance, leads to the change in optical wavelength expressed in terms of $\nu(k)$,

$$\Delta\nu(k) = \nu(k) - \nu_o = -\frac{d\phi}{dz}, \tag{3.3}$$

where z is the dimensionless distance normalized to $N\lambda$. This equation relates the slope of the optical phase along z to the change of the optical wavelength expressed as $\Delta\nu(k)$ away from the resonance wavelength expressed as ν_o.

Figure 3-7 shows a series of snapshots of the optical phase $\phi(z)$ at equal intervals in one cycle of the electron beam energy modulation. These were made using $j = 1.5$, $d = 0.02$, $Q = 30$, $\sigma_z = 1.2$, $A = 0.5\pi$, and $\Lambda = 400$. The resonant frequency has been chosen at $\nu_o = 4.0$, allowing for better display of the optical phase. Referring to Figure 2-4, this value of ν_o is near the peak in the gain curve for strong fields. This value of ν_o will give less severe changes in the slope $d\phi/dz$, but still allow a valid simulation that can change frequency in any manner.

At the top is the optical pulse $|a(z)|$, whose basic shape remains approximately the same throughout the evolution and is shown for reference. On the bottom is the electron pulse shape also shown for reference. In the middle are five snapshots of the optical phase $\phi(z)$, the top at $n = 1200$ and the bottom at $n = 1600$ in intervals of 100 passes. On the right is shown the optical power evolution $P(n)$, annotated over one period of the electron beam energy modulation, and the optical power spectrum $P(\nu)$ corresponding to each $\phi(z)$ curve. The optical line center in $P(\nu)$ can be seen to move back and forth along the ν axis as the optical field responds to the changing resonant wavelength.

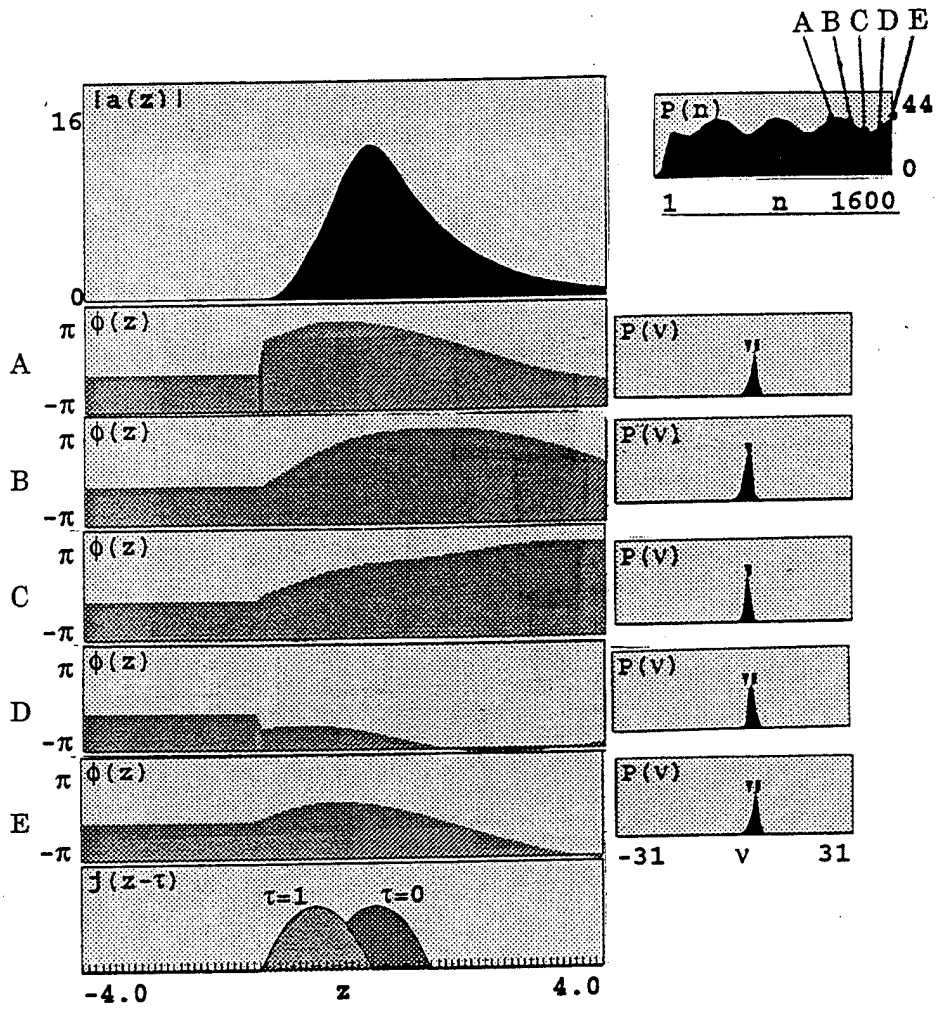

Figure 3-7. Optical phase progression. Electron beam energy modulation can be followed through $P(\nu)$ and $P(n)$. Desynchronism moves new information to the right along the optical pulse $|a(z)|$.

In the top optical phase plot, labeled A, the region to the left of the optical pulse contains no optical field and the phase has a constant value of zero. Moving to the right along z, there is a region with positive slope, indicating decreasing wavelength from ν_o, followed by a region of nearly constant negative slope, which indicates increasing wavelength from ν_o. This is because the change in $\nu(k)$ is the negative of the slope $d\phi/dz$. Correspondly, the left-most portion of the optical pulse has frequencies which are increasing and the rest has decreasing frequencies. Since this right-most portion has a nearly constant slope, the wavelength decrease is fairly uniform over this area of the optical pulse. $P(\nu)$ is near its farthest point to the right along the ν axis, since most of the optical phase at this point has negative slope.

Moving to the optical phase plot labeled B, the maximum in the optical phase curve has shifted to the right. The transfer of information from electrons to the optical pulse occurs in the region of the optical pulse directly above $\tau = 1$ of the electron pulse diagram. Over many passes, this information moves forward along the optical pulse through desynchronism. This is expressed as $\Delta z \approx d\,\Delta n$. Since the optical pulse is about $z = 4$, it will take about 200 passes with $d = 0.02$ for information to traverse the optical pulse, or about half the period of the electron beam energy modulation. Optical phase diagram B is 100 passes after the previous one, and the maximum in the optical phase curve has moved about half way across the optical pulse. $P(n)$ shows the electron beam energy modulation has progressed a quarter period. Although desynchronism has moved the maximum of the optical phase along the optical pulse, the electron beam energy modulation is decreasing the resonant wavelength at the beginning of the optical pulse, as denoted by $d\phi/dz$ being positive here. $P(\nu,n)$ is shifting left in response to this.

Optical phase plot C is 200 passes after plot A, and the maximum in the optical phase has moved to the end of the optical pulse. The optical phase has a nearly constant negative slope, which means all the frequencies in the optical pulse are shifting to lower values. Desynchronism is changing the frequencies on the right and energy modulation of the electrons is changing frequencies in the interaction region above the electron pulse envelope at $\tau = 1$. $P(n)$ has reached half of its cycle, and $P(\nu,n)$ has shifted to near its left-most position on the ν axis.

In optical phase plot D, the maximum in the optical phase is near the beginning of the optical pulse, ready to move to the right through desynchronism. The optical phase plot has shifted lower along the ϕ axis, but this is due to another phase in the system which doesn't affect the relationship, $d\phi/dz$, so the vertical shift is of no consequence here. $P(n)$ is three quarters through its cycle, and $P(\nu)$ is approaching its right-most maximum from the left.

In the final optical phase plot, the overall shape of $\phi(z)$ is the same as in the top plot, indicating that the electron energy beam modulation is has repeated itself. This is verified by noting that $P(n)$ has returned to its original position along n.

D. LIMIT CYCLE BEHAVIOR WITH SMALL AMPLITUDE MODULATIONS

Figure 3-9 displays limit cycle behavior. A peak optical field of $|a(z,n)| \approx 32$ has become sufficient to trap electrons in the potential wells caused by the optical field. The electrons have begun to orbit the phase space fixed point of $(\zeta,\nu) = (\pi/2,0)$ and although they don't complete a full synchrotron orbit in one pass, the potential wells are deep enough so that the electrons execute a large part of a synchrotron orbit and the limit cycle behavior is present. Sidebands have formed

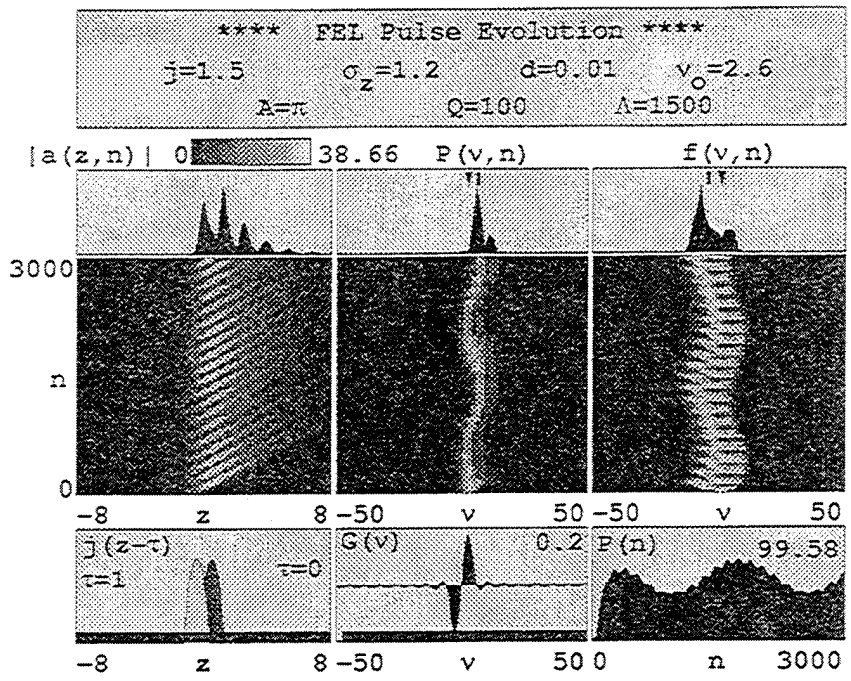

Figure 3-8. Limit cycle behavior causes submodulations in $P(n)$.

at $\nu \approx \nu_o \pm \nu_s$ where $\nu_s \approx \sqrt{a} \approx \sqrt{32} \approx 2\pi$ and are apparent in the final optical power spectrum $P(\nu,z)$ in the top center plot.

Taking a value of $n = 500$ on the optical field plot $|a(z,\nu)|$, where the optical pulse has grown to its maximum width, and then moving up the plot as n increases, the peaks in the optical field move to the right along the z axis with increasing n. This movement of subpulses along the optical pulse cause the area under the optical field envelope to change, which results in the submodulations in the peak power $P(n)$ as n increases.

E. MODULATION OVER MANY FREQUENCIES

The ability of a FEL to follow the modulation of the electron beam energy modulation over a range of frequencies is examined by tracking the centroid of the

optical power spectrum $P(\nu)$ over many passes. The ratio of the maximum change in the centroid of the optical power spectrum to the electron beam energy modulation is,

$$\frac{\nu_c}{A} = \frac{\int \nu P(\nu) d\nu}{\int P(\nu) d\nu}. \tag{3.4}$$

Figure 3-9 shows the tracking of the centroid over a range of frequencies. On the vertical axis is the ratio of the maximum change in the amplitude of the centroid frequency to the amplitude of the electron beam energy modulation. In these runs,

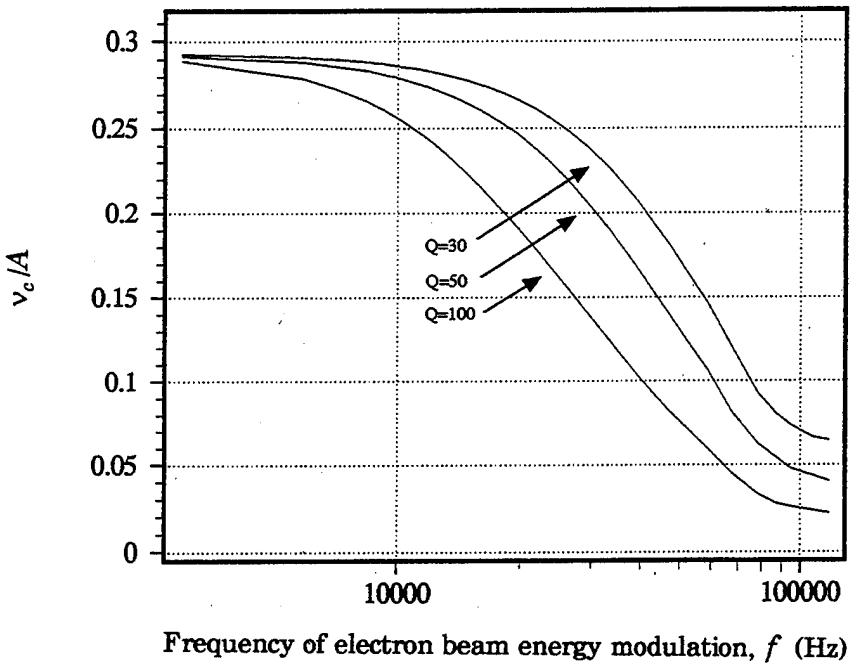

Figure 3-9. Decreasing the loss factor Q moves the curve ν_c/A to the right and changes the rate of roll-off.

the electron beam energy modulation is $A = 0.1\pi$, so that a ratio on the vertical axis of $\nu_c/A \approx 0.314$ would correspond to the FEL following the electron beam energy modulation perfectly. Desynchronism is $d = 0.02$, dimensionless beam current is $j = 1.5$, and the dimensionless electron pulse length is $\sigma_z = 1.2$. Using

different values of the loss factor Q results in different roll-off points and varying shapes of the roll-off curves along the frequency axis. The FEL is able to follow the electron beam energy modulations to higher frequencies as the loss factor Q was decreased, as shown by the curves moving to the right with increasing Q. Less loss in the FEL corresponds to the optical information being kept in the resonator over more passes, with the result that the centroid of the optical power spectrum is slower to respond to the newer information from the changing electron beam energy modulation.

The manner in which the roll-off occurs is different as well. The roll-off occurs more rapidly for the smaller loss factor and seems to begin leveling out at a higher ratio of ν_c/A. With the resolution of the numerical techniques in use here, the information above $f \approx 107$ kHz becomes unreliable, but the curves appear to approach a ratio of $\nu_c/A = 0$ asymptotically. Since $\Lambda = c/(2Sf)$, this corresponds to a period of $\Lambda \approx 100$.

Figure 3-10 displays the results of manipulating the desynchronism factor d of the FEL over a range of frequencies. Although the shapes of the curves remain similar with changing d, there is a shift to the right with increasing desynchronism, corresponding to the FEL following the electron beam energy modulations to higher frequencies with increasing d. Increasing desynchronism increases the length of the optical pulse, and increases the rate at which optical information moves to the right along z over many passes. As the electron pulse changes the resonant optical frequency at the trailing edge of the laser pulse, the desynchronism process distributes the new light to the right. For large values of d, the new light at a new frequency spreads more rapidly. The FEL more easily follows at larger values of desynchronism d.

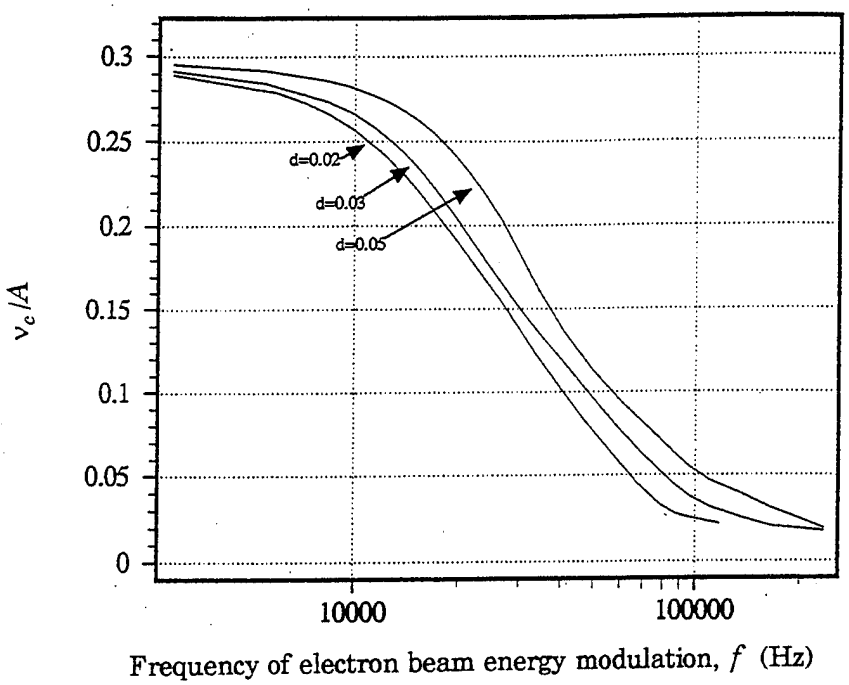

Figure 3-10. Increasing the desynchronism d moves the curve ν_c/A to the right such that the FEL will roll-off at a higher frequency of electron beam energy modulation, f.

Figure 3-11 shows ν_c/A (as a solid line) for reference, describing how the optical power follows the electron beam modulation at lower frequencies, f. The fractional change $\Delta P(n)/P(n)$ in the oscillating optical power is shown as a dashed line. At lower frequencies f, the optical power spectrum follows the changing resonance frequency, so that the optical power modulation $\Delta P(n)/P(n)$ is small. As the modulation frequencies are increased, the average power $P(n)$ decreases since the FEL isn't as efficient at following the resonant frequency. The modulation in the output power reaches a maximum at $f \approx 65$ kHZ. Above that frequency, the amplitude of the output power modulation begins to fall, as the light pulse begins to struggle to keep up with the rapidly changing resonant frequency. The amount of maximum power modulation occurs when the ratio $\Delta\nu_c/A$ is about 50%.

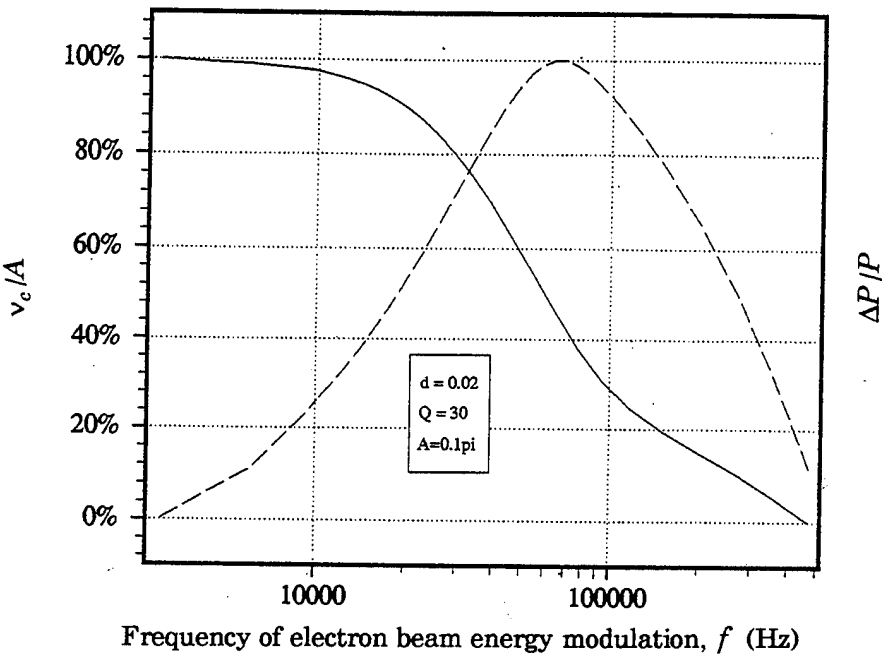

Figure 3-11. A comparison of the roll-off of v_c/A (solid line) to the relative amplitude of modulation in the output power P (dashed line).

IV. CONCLUSIONS

The FEL has a potential for use as a weapon in the US military arsenal, not only for use against anti-ship missiles and theatre ballistic missiles, but in other roles as well. The tunability of the FEL over a wide range of wavelengths at high powers make it an attractive candidate for a variety of uses. Chemical lasers are currently in the limelight of consideration for many of these applications, but further advances in FEL design and technology will necessitate more thought as to the implementation of the FEL. Certainly, land-based FEL's for use in the theatre ballistic missile defense would be more easily developed than a FEL for shipboard use. But current anti-ship missile design is already pushing the capability of the anti-missile defenses in place today. Counter measures against a fixed wavelength weapon could be defeated by a tunable FEL. The future may see the need for a flexible answer to this threat, and the FEL may be the answer.

Work at the Stanford SCA has been directed towards the problem of wavelength stabilization in the FEL through the use of feedback mechanisms to control the electron beam energy before it enters the undulator. It is hoped that methods such as this will allow more stable output from the FEL for use in other experiments being conducted. Using numerical methods, a simulation of the fundamental process of resonant wavelength modulation has been created to study the relation between a modulating electron beam and the output optical power.

Variance of such parameters as desynchronism, the resonator loss factor Q, and the frequency of the electron beam modulation have different effects on the output power from a short pulse FEL and its ability to follow these modulations. It is seen that varying these parameters at an amplitude of modulation within the gain bandwidth of the FEL has much the same effects as if the modulations were outside the gain bandwidth. A decrease in resonator loss and an increase in

desynchronism both allow the FEL to follow the resonant wavelength shifts to higher frequencies of electron beam energy modulation. The manner in which these effects occur over a range of frequencies also depends on change in the above mentioned parameters. Roll-off occurs more quickly at lower values of the resonator loss factor.

LIST OF REFERENCES

[1] J. Albertine, Dir. Navy High Energy Laser Program, guest lecturer at Naval Post Graduate School Colloquium, (1994).

[2] J. Boatman and M. Hewish, "Naval Mine Countermeasures," Intl. Def. Rev. 7, (1993).

[3] C. A. Brau, "Free-Electron Lasers," pp. 3-6, (Academic Press, Inc., San Diego, CA, 1990).

[4] J. M. J. Madey, J. Appl. Phys. 42, 1906 (1971).

[5] W. B. Colson, Phys Lett. 59A, 187 (1976).

[6] W. B. Colson, "Simulation of Free Electron Lasers," Proc. SPIE, 1045, 2-9 (1989).

[7] W. B. Colson, "Classical Free-Electron Laser Theory," in Laser Handbook, W. B. Colson, C. Pellegrini and A Reneiri, Volume 6, (North Holland, Amsterdam, NE, 1990).

[8] A. Marziali, T. I. Smith, "Feedback Stabilization of the SCA/FEL Wavelength," Nuc. Instr. and Meth. A, 331, 59 (1993).

INITIAL DISTRIBUTION LIST

1.	Defense Technical Information Center Cameron Station Alexandria, Virginia 22304-6145	2
2.	Dudley Knox Library, Code 52 Naval Postgraduate School Monterey, California 93943-5101	2
3.	Professor William B. Colson, Code PH/Cw Chairman, Department of Physics Naval Postgraduate School Monterey, California 93943-5117	6
4.	Professor Robert Armstead, Code PH/Ar Department of Physics Naval Postgraduate School Monterey, California 93943-5117	1
5.	Lieutenant W.R. Pinkley, USN 586 Queens Mirror Circle Casselberry, Florida 932707	2